nature communications

Article

https://doi.org/10.1038/s41467-025-62119-9

Nanoscale fletching of liquid-like polydimethylsiloxane with single perfluorocarbons enables sustainable oil-repellency

Received: 11 March 2025

Accepted: 10 July 2025

Published online: 23 July 2025

Check for updates

Samuel Au[1], Jeremy R. Gauthier[2], Boran Kumral[1], Tobin Filleter[1], Scott Mabury[2] & Kevin Golovin[1]

Oil repellency is essential for enabling self-cleaning, anti-soiling and stain-repelling properties, which has broad application in industries liked textiles, healthcare and electronics. While per-and-polyfluoroalkyl substances (PFAS) exhibits strong oleophobicity, their environmental and health risks have led to prohibition on long-chain PFAS ($\geq C_8$) and restriction on short-chain PFAS (C_4, C_6). However, there are few alternative materials demonstrating comparable oil repellency. Here, we introduce a novel method to fletch polydimethylsiloxane (PDMS) brushes with ultrashort PFAS (singe -CF_3, the least toxic PFAS), achieving oil repellency similar to short-chain PFAS while drastically reducing the fluorine content. This work highlights that liquid-like molecular design, rather than chain length, can enable sustainable oil repellency, facilitating a smoother transition away from PFAS reliance.

Perfluoroalkyl substances (PFAS) are conventionally used to fabricate omniphobic coatings, which can passively repel liquids of both high surface tension (e.g., water) and low surface tension (e.g., oils), and are broadly applicable in microfluidics[1,2], condensation[3–5], membrane technology[6–8], anti-fouling[9,10] and anti-icing[11–13]. PFAS can be categorized as C_L, where L is the total number of fluorinated carbons along the alkyl chain, and thus different chain lengths of PFAS may be grouped together, including long chain ($\geq C_8$), short chain (C_6–C_4) and ultrashort chain (C_1–C_3) PFAS[14]. Longer chain PFAS have been shown to demonstrate greater liquid repellency due to the self-assembly of the fluoroalkyl chains, forming a crystalline or semi-crystalline self-assembled monolayer (SAM) which maximizes the surface density of the terminal trifluoromethyl group (-CF_3)[15]. The surface density of -CF_3 groups determines the surface energy, where a closely packed -CF_3 surface exhibits the lowest surface energy humans have produced to date, ~6 mN/m[16]. However, the toxicity and bioaccumulation of PFAS is reported to increase with the length of the fluorocarbon chain[17,18], and therefore the use of long-chain PFAS ($\geq C_8$) has already been restricted in many countries. Numerous studies[19–24] have supported the work of Luz et al., where they state, "short-chain [PFAS], as compared to long-chain [PFAS], are more quickly eliminated from mammals via urinary excretion… the French Agency for Food, Environmental and Occupational Health & Safety (ANSES) proposed a human health chronic oral toxicity value (0.32 mg/kg·day) for [C_6 PFAS in 2024] that is more than four orders of magnitude greater (i.e., less toxic) than the oral toxicity value derived by the U.S. Environmental Protection Agency (USEPA) for the drinking water health advisory for PFOA [(C_8 PFAS)], (0.00002 mg/kg·day)."[25] However, while short chain (C_6–C_4) and ultrashort chain PFAS (C_1–C_3) are currently being utilized as an alternative to long-chain PFAS, their reduced crystallinity results in weaker liquid repellency. Moreover, short-chain PFAS shares similar mechanisms of toxicity with their long-chain counterparts, such as peroxisome proliferation that can lead to liver toxicity[25,26]. As a result, a proposed EU-wide regulation on all PFAS is being reviewed[27], indicating an urgent need for the replacement of PFAS.

[1]Department of Mechanical and Industrial Engineering, University of Toronto, Toronto, ON, Canada. [2]Department of Chemistry, University of Toronto, Toronto, ON, Canada. e-mail: kevin.golovin@utoronto.ca

Here we take inspiration from perfluoropolyethers (PFPE)[28], which are comprised of repeating units of ultrashort chain PFAS (C_2 and C_3) connected by an ether backbone (C-O-C), and specifically PFPE in the polymer brush conformation. In this conformation chains are covalently bonded to the surface on one end, while the rest of the polymer is still able to stretch, rotate and bend freely, exhibiting many features of a liquid lubricant[29]. Although PFPE brushes do not self-assemble due to their low glass transition temperature[29], the flexibility of the ether linkage allows for the thermodynamic re-orientation of the C_2 and C_3 fluoroalkyl chains to the outermost surface, which can also maximize the surface density of -CF_3 groups[28]. Due to this re-orientation, PFPE brushes demonstrate strong omniphobicity comparable to short chain PFAS[4,30,31]. Further, if PFPE brushes are degraded the chain is truncated into shorter and shorter PFPE chains and eventually only ultrashort chain PFAS (C_2 and C_3), which are comparably of less concern to environmental contamination and human exposure than short and long chain PFAS according to the current understanding of PFAS toxicity. However, not only does PFPE still contain a substantial amount of PFAS, the majority of the perfluorinated polymer does not end up on the outermost surface as it is chemically bound to the polymer backbone. This suggests that most of the PFAS within PFPE is excessive and will eventually lead to unnecessary PFAS emissions without notable benefit in terms of omniphobicity.

The above indicates that long fluoroalkyl chains are not necessary to enhance the surface density of -CF_3. In fact, Urata et al.[32,33] had shown that a polymer chain containing a single -CF_3 (C_1) side group can repel oils with surface tension as low as 23.8 mN/m (i.e., *n*-decane). With the current understanding of short-chain PFAS toxicity[26], shorter PFAS presents lower toxicity in terms of the peroxisome proliferation, its effect on lipids, cytotoxicity, and neurotoxicity, and therefore a single -CF_3 group is the least toxic of any PFAS. Moreover, one of the terminal degradation products of a single -CF_3 group is trifluoroacetic acid, which has been reported to be excreted from mammals easily without bioaccumulation and poses very low toxicity to aquatic life[34]. Furthermore, the use of single -CF_3 groups has vast application in different chemical designs. For example, single -CF_3 groups are present in many FDA approved pharmaceuticals including Riluzole (myotrophic sclerosis), Delamanid (tuberculosis), Sonidegib (cancer), Pretomanid (tuberculosis), and Celikalim (blood pressure)[35]. In addition to pharmaceutical applications, single -CF_3 groups are also widely used in various material designs, including solar cells[36] and fluorescence microscopy[37]. As a result, with proper surface design, coatings utilizing a single -CF_3 group have a strong potential for omniphobicity and as a replacement to current PFAS materials, but with significantly reduced impacts on environmental sustainability and human health.

Going one step further, many researchers have investigated completely fluorine-free omniphobic coatings. Polydimethylsiloxane (PDMS) brushes have been explored as a promising non-PFAS alternative[38–41]. PDMS brushes are comprised of a long siloxane chain decorated with relatively low surface energy methyl side groups (-CH_3). Similar to the migration of -CF_3 within PFPE brushes, the surface energy of PDMS brushes is minimized through the migration of -CH_3 to the outermost surface. However, the repellency of low surface tension oils on PDMS brushes is still weaker than short chain PFAS due to the large difference between the surface energy of -CH_3 (~19–22 mN/m) and -CF_3 (~6 mN/m). To bridge this gap, here we propose to incorporate several single -CF_3 groups (i.e., no alkyl chain) onto PDMS brushes to reduce their dispersive surface energy and thus improve their liquid-repellent properties. We demonstrate that the oil repellency of PDMS brushes can be significantly enhanced by rationally replacing silanol and methyl groups with several single -CF_3 groups at the end of PDMS brushes. However, here the flexibility of the PDMS brushes enables a high surface density of -CF_3 groups without excessive perfluorination that does not contribute to the surface properties. Angle-resolved XPS reveals that the molecular distribution of such -CF_3 groups is similar to the feathers used to fletch the end of an arrow, and we therefore refer to such chemical modification as "CF_3 fletching". CF_3-fletched PDMS brushes exhibit a dispersive surface energy approaching that of short chain C_6 PFAS, which enables the repellency of low surface tension oil droplets including heptane, which completely wets conventional PDMS brushes. Moreover, the fluorine surface density of CF_3-fletched PDMS brushes (~10 F/nm^2) is 8 times lower than that of monofunctional C_6 PFAS (~78 F/nm^2) and ~40 times lower than that of a trifunctional C_4 PFAS (~406 F/nm^2) which exhibits comparable liquid-repellent properties. This indicates that CF_3-fletched PDMS brushes not only would release the least harmful type of fluorocarbon (a single -CF_3 group) but also would emit a significantly smaller amount of fluorocarbon into the environment. This study demonstrates that single -CF_3 groups can result in omniphobic surfaces through the rational modification of PDMS brushes.

Results

Fabrication and characterization of CF_3 fletched PDMS brushes

The fabrication process of CF_3 fletched PDMS brushes is illustrated in Fig. 1a. First, PDMS brushes were grown on a cleaned silicon wafer as described in our previous work[38] (see detailed process in the Supplementary Methods). The thickness of the PDMS brush layer was 3.5 ± 0.3 nm as measured by ellipsometry (see Supplementary Note 2), consistent with prior literature values[38]. Inspired by recent work generating branched PDMS brushes[42], the PDMS brushes were then treated with oxygen plasma for 15 s to partially convert surface methyl groups to silanols. After plasma treatment, a CF_3 fletching agent (3,3,3-trifluoropropyldimethylchlorosilane) was used to replace these silanols with one or more single -CF_3 groups. See *Methods* for the details of the surface fabrication process.

The oil repellency of the CF_3-fletched PDMS brushes was then compared to methyl capped PDMS brushes and a self-assembled monolayer (SAM) formed from the CF_3-fletching agent (see *Methods* for synthesis details). The advancing contact angles, θ_{adv}, of several low surface tension, σ_l, alkane oils – including hexadecane (σ_l = 27.47 mN/m), tetradecane (26.56 mN/m), dodecane (25.35 mN/m), decane (23.83 mN/m), octane (21.62 mN/m) and heptane (20.14 mN/m) – were measured on these three surfaces (Fig. 1b). The advancing contact angles of the CF_3 fletched PDMS brushes were consistently higher than those of the methyl-capped PDMS brushes and the CF_3 fletching agent SAM for all oils evaluated, with an average increase of ~10°. These results confirm the migration of the low surface energy -CF_3 group to the surface of the PDMS brushes, enabled by their liquid-like properties[43]. In addition, atomic force microscopy (AFM, see Supplementary note 5) indicated that the root-mean-square roughness S_{rms} of the CF_3-fletched PDMS brushes (S_{rms} = 0.48 ± 0.09 nm) was statistically equivalent to that of the PDMS brushes (S_{rms} = 0.33 ± 0.08 nm) without CF_3 fletching. Wenzel roughness values of both the PDMS brushes (≈1.0005) and CF_3 fletched PDMS brushes (≈1.0010) were also calculated from AFM topography data. These values suggest that CF_3 fletching did not influence the surface roughness of PDMS brushes and that roughness does not explain the wettability changes observed after fletching the PDMS brushes with -CF_3 groups.

The surface chemistry of the PDMS brushes before and after CF_3 fletching was explored using X-ray photoelectron spectroscopy (XPS, see Supplementary note 4). Fig. 1c shows the XPS survey spectra of the PDMS brushes before and after CF_3 fletching. The presence of the F 1 s peak at ~689.0 eV[44] in the CF_3-fletched PDMS brush spectrum indicates the addition of fluorocarbon resulting from CF_3 fletching. To confirm that the added fluorocarbon was solely trifluoromethyl groups (-CF_3), the C 1 s spectrum was also analyzed (Supplementary Fig. 2, Supplementary note 3). The C 1 s peak at approximately 293.5 eV corresponds to -CF_3, with no indication of a -CF_2- peak near 292 eV[45], confirming that

https://doi.org/10.1038/s41467-025-62119-9

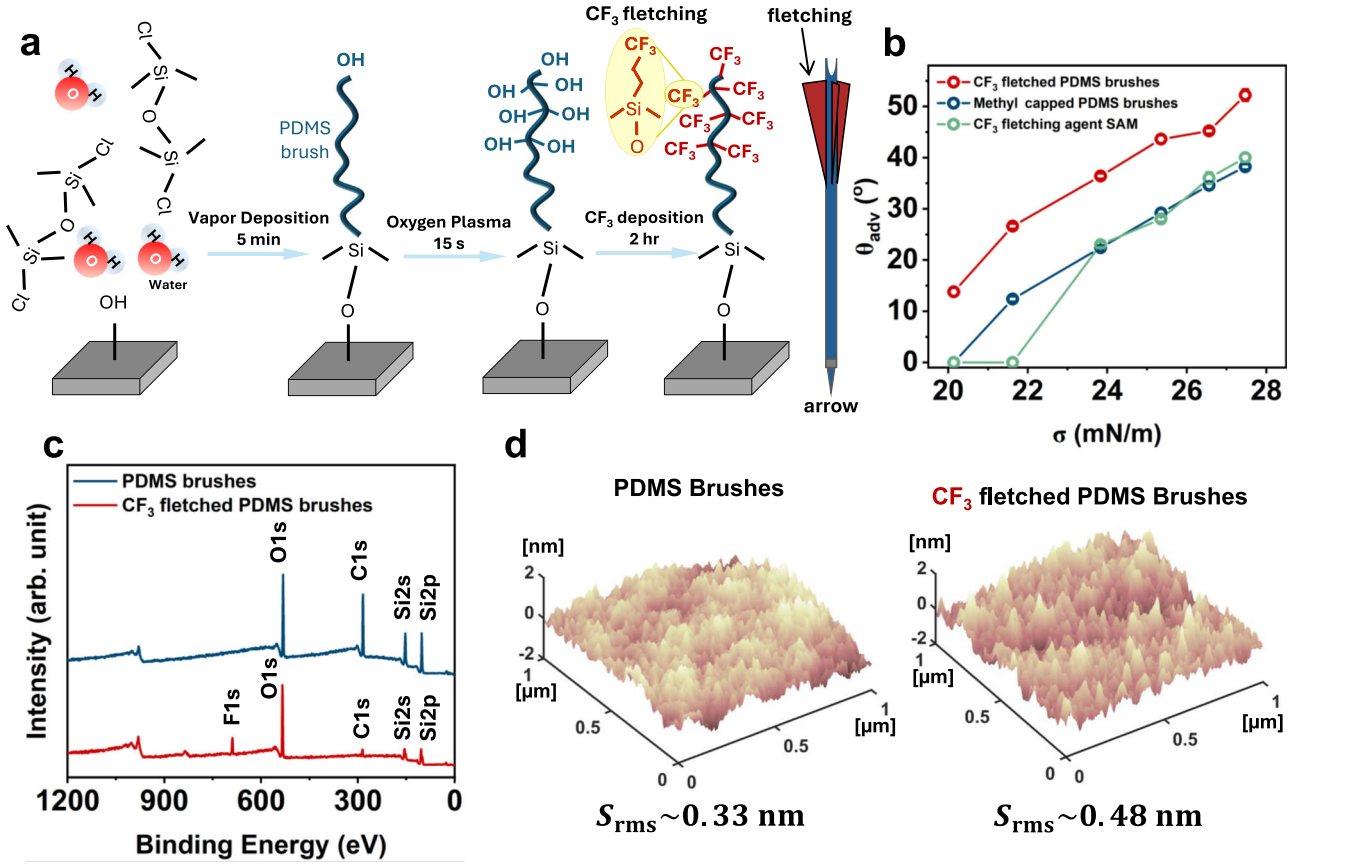

Fig. 1 | Fabrication and characterization of CF_3 fletched PDMS brushes. **a** Schematic illustration of the fabrication process of the CF_3 fletched polydimethylsiloxane (PDMS) brushes. **b** The advancing contact angles θ_{adv} plotted against surface tension σ_l for several low surface tension oils on CF_3 fletched PDMS brushes, methyl capped PDMS brushes, and the CF_3 fletching agent self-assembled monolayer (SAM). Here $N = 5$ and the data is the mean ± 1 std. **c** X-ray photoelectron spectroscopy (XPS) survey spectra for the PDMS brushes and the CF_3 fletched PDMS brushes. **d** Surface topography of the PDMS brushes and the CF_3 fletched PDMS brushes probed by atomic force microscopy (AFM), with the root-mean-squared roughness (S_{rms}) shown.

no fluorocarbon chain formed and that one or more single -CF_3 groups were the only fluorocarbons present.

Omniphobicity of CF_3 fletched PDMS brushes

To investigate how liquid repellency varied with the amount of CF_3 fletching agent bonded to the PDMS brushes, the plasma treatment time t_p of the PDMS brushes was controlled from $t_p = 0$ s (no plasma treatment) to $t_p = 30$ s. The surface fraction of silanols (Si-OH) on the PDMS brushes immediately after plasma treatment was estimated via water wettability measurements and the molecular Cassie-Baxter equation[46] (Supplementary Fig. 1, Supplementary note 3). Similar to the plasma treatment of PDMS-based elastomers[47], the surface fraction of silanols on PDMS brushes increased with the plasma treatment time, with a sufficient number of surface methyl groups converted to silanols after $t_p = 15$ s to cause complete wetting by water.

Following the vapor deposition of the CF_3 fletching agent on all PDMS brush samples, from no plasma treatment ($t_p = 0$ s) to 30 s of plasma treatment, the samples were analyzed using XPS to examine their surface chemical composition. The fluorine-to-siloxane atomic ratio, F/SiO_2C_2, was utilized to monitor the amount of CF_3 groups added to the PDMS chains (see Supplementary Table 2 and Supplementary note 4 for validation) and is plotted against plasma treatment time in Fig. 2a. For the $t_p = 0$ s surface, the CF_3 fletching agent bonded to the preexisting terminal silanols of the PDMS brushes, the presence of which we recently confirmed[38,48]. The F/SiO_2C_2 atomic ratio was found to increase with the plasma treatment time due to the increasing amount of silanols generated and available for reaction with the CF_3 fletching agent (Supplementary Fig. 1). Although the surface fraction of silanols approached 100% at $t_p = 15$ s, the F/SiO_2C_2 ratio continued to increase significantly after this point (Fig. 2a). This increase may be attributed to the conversion of methyl groups into silanols beneath the uppermost surface (recall that the PDMS brushes here are ~3.5 nm thick with a degree of polymerization around 100)[38,48]. These additional silanols can potentially also be fletched by the CF_3 fletching agent, resulting in a subsequent increase in the F/SiO_2C_2 ratio.

To estimate the average number of CF_3 groups bonded to each PDMS chain, we first assume that the CF_3 fletching agent can react with most of the single silanol groups terminating the PDMS brushes not treated with plasma. We set the fluorine-to-siloxane atomic ratio measured for this sample ($F/SiO_2C_2 \approx 0.0350$) as reference value n_1, i.e., one CF_3 fletching agent bonded to one PDMS brush. As a result, the number of CF_3 fletching agents n on the plasma treated PDMS brush can be estimated by dividing their fluorine-to-siloxane atomic ratio by n_1. The estimated number of CF_3 fletching agent molecules bonded to the plasma-treated PDMS brush surfaces are shown on the right axis in Fig. 2a. For 30 s of plasma treatment, we estimate ~10 CF_3 fletching molecules were bonded to each PDMS brush.

The advancing and receding contact angles of hexadecane were also measured for these CF_3-fletched PDMS brushes and are plotted against the plasma treatment time in Fig. 2b. Both the advancing and receding contact angle of hexadecane increased with the plasma treatment time and the fluorine-to-siloxane atomic ratio, confirming that adding the CF_3 fletching agent to the PDMS brushes improves the surface's ability to repel low surface tension fluids. However, while the advancing contact angle of hexadecane plateaued after a plasma treatment time of $t_p = 15$ s, the fluorine-to-siloxane atomic ratio

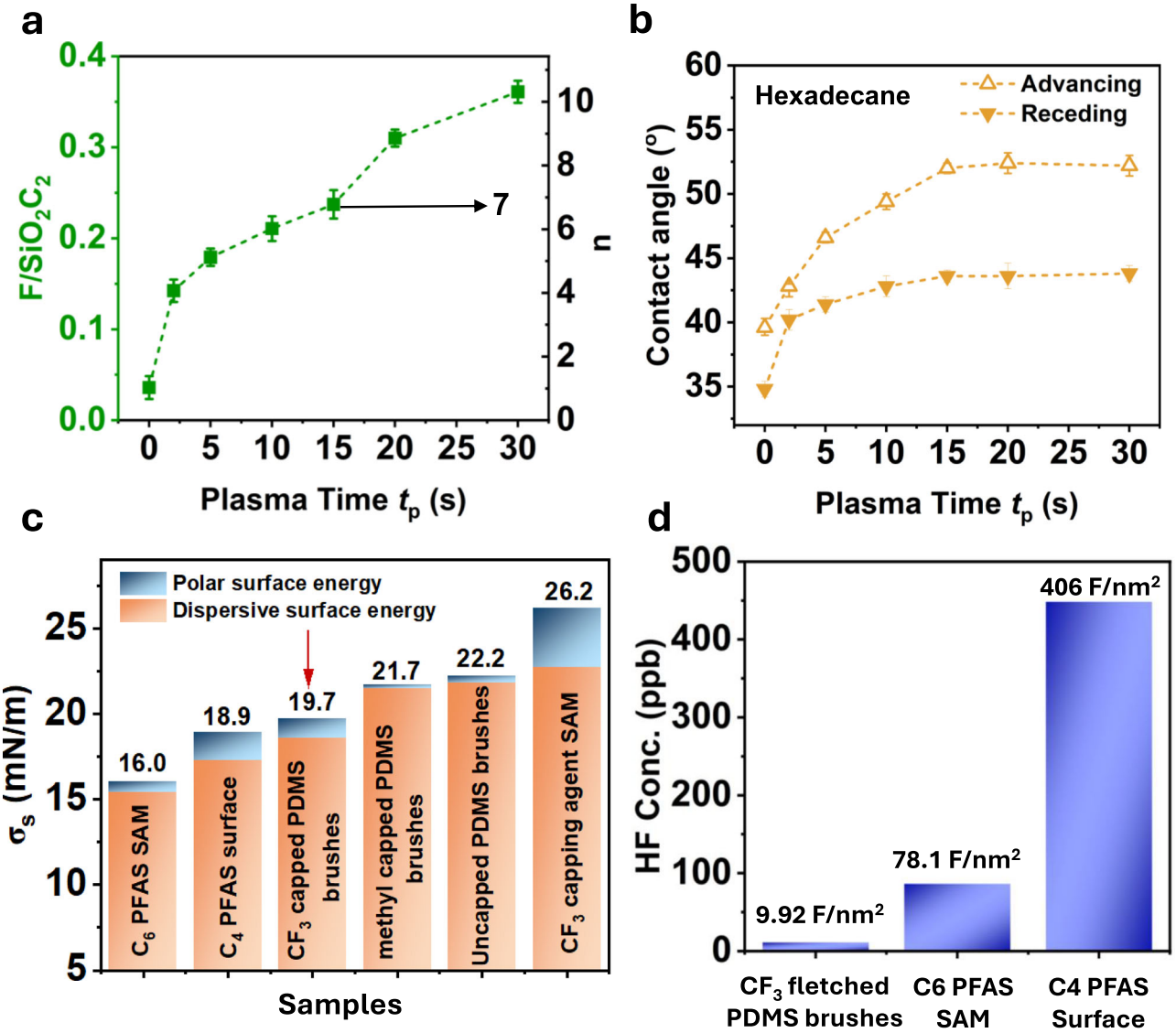

Fig. 2 | Fluorine content and oil repellency of CF_3 fletched PDMS brushes. a The fluorine-to-siloxane atomic ratio F/SiO_2C_2 as a function of the plasma treatment time t_p and estimated number of bonded CF_3 fletching agents n. See Supplementary Information Supplementary Note 4 for a discussion on the uncertainty calculations. Data ($N = 5$) are presented as mean values ± 1 std. **b** The advancing and receding contact angles of hexadecane on the CF_3 fletched PDMS brushes as a function of the plasma treatment time t_p prior to CF_3 fletching. Here $N = 5$ and the data is the mean ± 1 std. **c** The total surface energies for surfaces considered in this work, calculated using the OWRK method. **d** The absolute surface density of fluorine for the CF_3 fletched PDMS brushes, C_6 PFAS SAM and C_4 PFAS surface measured via ToF-CIC.

continued to increase. This indicated that the additional CF_3 fletching molecules were reacting with non-surface silanols that did not contribute to surface wettability. Accordingly, the surface density of -CF_3 groups was maximized after 15 s of plasma treatment, resulting in a hexadecane advancing contact angle of 52 ± 0.1°. Note that this is much larger than the measured hexadecane advancing contact angle on PDMS brushes (37 ± 0.5°) and methyl capped PDMS brushes (40 ± 0.5°). From the F/SiO_2C_2 ratio, 7 CF_3 fletching molecules were bonded to these PDMS brushes (Fig. 2a), resulting in the proposed structure shown schematically in Fig. 1a. To confirm this structure, angle resolved XPS was performed on the CF_3 fletched PDMS brushes treated with 15 s of plasma in order to probe the chemical composition at different depths by varying the electron take-off angle $\theta_{take-off}$ from 10° to 90° (see Supplementary Information Supplementary note 4 for details). Supplementary Fig. 4 plots the F/SiO_2C_2 ratio as a function of $\sin(\theta_{take-off})$, which is directly proportional to the probe depth. The fluorine-to-siloxane atomic ratio decreased dramatically with increasing $\sin(\theta_{take-off})$, indicating that most of the CF_3 fletching agents were located at the top surface of the PDMS brushes.

Despite of the significant increase in hexadecane contact angles, the addition of the CF_3 fletching agent reduced the advancing water contact angles from 106 ± 0.6° (PDMS brushes alone), to 101 ± 0.5° (CF_3 fletched PDMS brushes) (see Supplementary Table 1). This can be explained by the presence of a dipole moment at the hydrocarbon-fluorocarbon -CH_2-CF_3 junction formed by the CF_3 fletching agent[15,49]. This induced dipole moment can increase the polar surface energy component of the solid surface which would increase the surface's polar interactions with water molecules, reducing the advancing contact angle. For nonpolar liquids like hexadecane this effect would be minimal, which agrees with the increase in hexadecane advancing contact angles observed with increasing CF_3 fletching agent (Fig. 2b)

The total surface energy σ_s of the CF_3 fletched PDMS brushes (15 s of plasma), was calculated by the Owens, Wendt, Rabel and Kaelble (OWRK) method using the measured advancing contact angle of water

and hexadecane (Supplementary note 6). For comparison, the total surface energies of PFAS surfaces, including a C_6 PFAS self assembled monolayer (SAM) and a C_4 PFAS surface, as well as the methyl-capped PDMS brushes, PDMS brushes, and a SAM formed by the CF_3 fletching agent, were also calculated. Contact angles are listed in Supplementary Table 1, and the detailed fabrication processes are illustrated in the Supplementary Methods. The surface energies of these six surfaces are plotted in Fig. 2c. Although the polar surface energy of the CF_3 fletched PDMS brushes is greater than that of the methyl-capped PDMS brushes, its total surface energy is lower. Further, the total surface energy of the CF_3-fletched PDMS brushes (19.7 mJ/m^2) is similar to that of the C_4 PFAS surface (18.9 mJ/m^2) and is closer to that of the C_6 PFAS SAM (16.0 mJ/m^2) compared to the methyl-capped PDMS brushes. These results support our initial hypothesis that perfluorinated alkyl chains are not necessary to maximize the surface density of CF_3 groups, which minimizes the surface energy.

The above indicates that an omniphobic surface was developed with performance similar to C_4 or C_6 PFAS, by attaching 7 CF_3 groups to the top of PDMS brushes treated with plasma for 15 s. The benefit of such a surface can be seen by considering its eventual emissions of perfluorinated species into the environment. To do this, total organic fluorine – combustion ion chromatography (TOF-CIC) was performed on the CF_3 fletched PDMS brushes, the C_6 PFAS SAM and the C_4 PFAS coating. This technique quantifies the total fluorine that could potentially be released by the surface into the environment, though the type of species will depend on the exact degradation pathway. In TOF-CIC, all carbon-fluorine bonds are broken, generating fluorine radicals which form HF in the hydrated flow-through gas. The concentration of captured HF can then be used to calculate fluorine surface density, Γ_F (Supplementary note 7). Fig. 2d shows the resultant concentration of the HF solution obtained from the analysis of the above three samples. The fluorine surface density of the CF_3 fletched PDMS brushes (Γ_F ~ 10 F/nm^2) was around eight times lower than that of the C_6 PFAS SAM (Γ_F ~ 78 F/nm^2) due to the lack of a long fluorocarbon chain. The C_4 PFAS surface exhibited the largest fluorine surface density (Γ_F ~ 400 F/nm^2) due to its trifunctional silane which can polycondense and form a much thicker perfluorinated layer. Recall, however, that the C_4 PFAS and CF_3 fletched PDMS brushes exhibited almost identical omniphobic properties, indicating that the same surface performance was achieved with 40 times less fluorine. Moreover, although more study is required to confirm the environmental impact of short chain PFAS, the release of C_6 and C_4 PFAS and their degradation by-products to the environment are reportedly toxic and bio-accumulative[26,50], and will become varied forms of PFAS which makes remediation difficult. On the other hand, the CF_3 fletched PDMS brushes will solely degrade to trifluoroacetic acid[51,52], a substantially safer, non-bioaccumulative and traceable compound.

Oil droplet mobility on CF_3 fletched PDMS brushes

Droplet mobility on CF_3 fletched PDMS brushes and methyl capped PDMS brushes was compared to determine whether the -CF_3 groups enhance the droplet mobility of low surface tension liquid droplets. For comparison, we first measured the contact angle hysteresis of a series of low surface tension oils, including tetradecane (σ_l = 26.56 mN/m), dodecane (25.35 mN/m), decane (23.83 mN/m), octane (21.62 mN/m) and heptane (20.14 mN/m) on both surfaces (Fig. 3c). While the CF_3 fletched PDMS brushes exhibited significantly larger advancing and receding contact angles compared to the methyl capped PDMS brushes, the contact angle hysteresis of the CF_3-fletched PDMS brushes was ~2° higher for all probe liquids. This slightly larger contact angle hysteresis indicated that oil droplets experienced a higher static friction to initiate movement on the CF_3 fletched PDMS brushes. This is possibly due to the heterogeneity of surface chemistry (both -CH_3 and -CF_3 groups are present)[53], but doesn't reflect the dynamic friction that controls how fast a droplet can be removed from a surface once in motion.

To investigate the dynamic friction of the low surface tension liquids on the CF_3 fletched and methyl capped PDMS brushes, their dynamic friction coefficient μ was also measured (see Supplementary note 8). Dynamic friction can be studied with droplet sliding experiments as shown in Fig. 3a, b, where μ can be derived from total frictional force F_f exerted on the sliding droplet. The dynamic friction coefficients for all the probe liquids on the CF_3 fletched PDMS brushes were significantly lower than those on the methyl capped PDMS brushes (Fig. 3d), indicating a higher droplet mobility on CF_3 fletched PDMS brushes. The lower dynamic friction coefficient observed for the CF_3 fletched PDMS brushes was likely due to the higher contact angles it can achieve for the low surface tension liquids, which results in a shorter contact line during droplet sliding. It has been reported that viscous dissipation dominates dynamic friction with increasing droplet sliding velocity[54–57], where hydrodynamic shear stress is highest near the contact line (i.e., wedge viscous force)[58,59]. Therefore, droplets adopting a shorter contact line on the CF_3 fletched PDMS brushes potentially experience reduced viscous dissipation in comparison to those on the methyl capped PDMS brushes, resulting in higher droplet mobility. This result indicates that although the contact angle hysteresis of the CF_3-fletched PDMS brushes was slightly greater than that of the methyl-capped PDMS brushes (Fig. 3c), which resulted in a lower static coefficient of friction, the higher absolute contact angles for low surface tension oils on the CF_3-fletched PDMS brushes enabled lower dynamic friction during sliding. This agrees with previous works on PDMS brushes, where methyl capping resulted in substantially lower dynamic friction coefficients, even for surfaces with identical contact angle hysteresis[38].

Oil spray test

The results within Fig. 3 highlight that low surface tension liquid droplets sliding on the CF_3 fletched PDMS brushes exhibit better mobility than the methyl capped PDMS brushes. This would have practical utility in various industrial applications such as organic Rankine cycles[60] and air conditioning technologies[61], where efficient removal of low surface tension condensate droplets is critical to increase system efficiency. We designed an oil spray test where the surfaces were subjected to a continuous spray of either decane, octane or heptane to further understand this performance (Fig. 4a, also Supplementary note 9). For comparison, the methyl capped PDMS brushes, C_6 PFAS SAM, and CF_3 fletching agent SAM were analyzed in addition to the CF_3 fletched PDMS brushes. From Fig. 4c it can be observed that only the CF_3 fletched PDMS brushes and C_6 PFAS SAM were able to maintain dropwise removal for all three liquids, while the methyl capped PDMS brushes and the CF_3 fletching agent SAM were completely covered by heptane and octane films (see Supplementary Movies 1 and 2). Although a single octane droplet could be shed from the methyl capped PDMS brushes with a receding contact angle > 0° (Fig. 3c), the surface still became flooded by an octane film. This was likely due to the higher dynamic friction coefficient of the methyl capped PDMS brushes (Fig. 3d), which prevented the droplet's receding velocity from overcoming the fluid flow rate. As a result, the droplet surface density increased, ultimately leading to the formation of an octane liquid film (Fig. 4c). This observation is similar the mechanism of dropwise-to-filmwise transition in condensation heat transfer phenomena, where a larger droplet contact radius increases the departure Bond number, facilitating the onset of filmwise condensation[5].

To determine each surface's steady state dryness under continuous oil spray we define the liquid surface coverage Φ as the ratio of area covered by liquid to the total surface area (Fig. 4b). A liquid surface coverage of $\Phi = 1$ (complete liquid film) was measured for heptane and octane, for the methyl capped PDMS brushes and the CF_3 fletching agent SAM (Fig. 4c). On the other hand, the CF_3 fletched PDMS brushes and the C_6 PFAS SAM maintained dropwise liquid repellency for all low surface tension liquids evaluated; their sufficient droplet removal rate

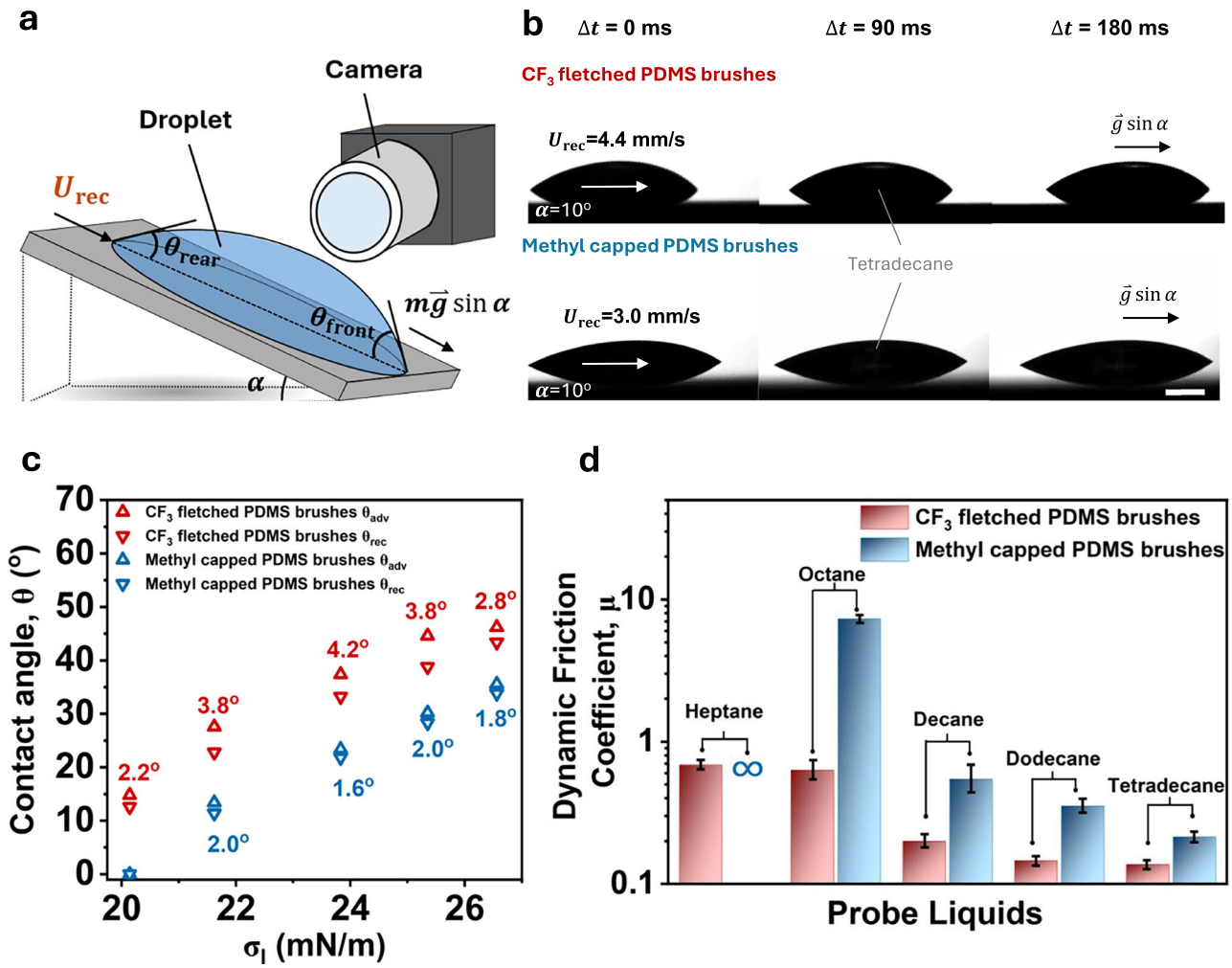

Fig. 3 | Dynamic friction of CF_3 fletched PDMS brushes. (**a**) Schematic illustration of the droplet sliding experiment. **b** Time-lapsed images of a 10 μL tetradecane droplet sliding on the CF_3 fletched and methyl capped PDMS brushes at a tilting angle of 10°. Scale bar: 1 mm. **c** Advancing and receding contact angles for CF_3 fletched and methyl capped PDMS brushes as a function of surface tension, for tetradecane, dodecane, decane, octane and heptane. The contact angle hysteresis is labeled next to each set of advancing/receding contact angles. Here $N = 5$ and the data is the mean ± 1 std. **d** The dynamic friction coefficient μ for CF_3 fletched and methyl capped PDMS brushes for different low surface tension liquids. For heptane, because the methyl capped PDMS brushes were completely wetted (i.e., $\theta_{adv} = \theta_{rec} = 0°$), the receding velocity was 0 mm/s for all tilting angles, resulting in an infinite dynamic friction coefficient (also see Supplementary Fig. 8). Here $N = 6$ and the data is the mean ± 1 std.

resulted in a significantly smaller value of Φ. The liquid surface coverage of the CF_3-fletched PDMS brushes was slightly higher than that of the C_6 PFAS SAM, which can be attributed to its slightly lower contact angles (Supplementary Table 1). Lower contact angles result in a larger droplet contact area, leading to increased liquid surface coverage. Regardless, these results highlight the importance of the dynamic friction coefficient rather than the contact angle hysteresis, in situations where the surface experiences continuous liquid deposition, because the rate of liquid removal will be limited by the droplet's receding velocity. Since the CF_3 fletched PDMS brushes exhibit a significantly lower dynamic friction coefficient compared to the methyl-capped PDMS brushes, Fig. 4 demonstrates their liquid repellency–on par with the C_6 PFAS SAM–in conditions necessitating the dropwise condensation of low surface tension fluids, such as in the field of refrigeration and cooling.

Application of CF_3 fletched PDMS brush on different materials for oil repellency

For the broad applicability of CF_3 fletched PDMS brushes they would need to be able to be deposited onto various substrate materials like metals and polymers. To achieve this we followed the work of Kahtir et al.[62], where an intermediary layer of silica is first coated onto a bare substrate prior to PDMS brush deposition (Supplementary Methods). As illustrated in Fig. 5a, coated substrates of polyester, nylon, and aluminum effectively shed droplets of various surface tensions and viscosities, including octane ($\sigma_l = 21.62$ mN/m, $\eta = 0.509$ mPa·s), hexadecane ($\sigma_l = 27.47$ mN/m, $\eta = 3.03$ mPa·s), and Kaydol 35 ($\sigma_l \approx 31$ mN/m[63], $\eta \approx 68.4$ mPa·s).

Many engineering surfaces requiring omniphobic properties are rough or porous. To investigate whether the CF_3 fletched PDMS brushes could also be applied to textured surfaces and improve their resistance to the penetration of low surface tension liquids, a stainless-steel mesh was coated by the CF_3 fletched PDMS brushes (Supplementary Methods, also Supplementary Fig. 10). For comparison, the stainless-steel meshes were also coated by the methyl capped PDMS brushes, the CF_3 fletching agent SAM, C_4 PFAS or the C_6 PFAS SAM. The advancing contact angles of water, Kaydol 35, hexadecane and tetradecane were then measured (Fig. 5c). The C_6 PFAS SAM coated mesh exhibited the highest advancing contact angles for each liquid, consistent with the contact angle measurements on silicon wafers (Supplementary Table 1). The CF_3 fletched PDMS brush-coated mesh displayed similar contact angles with the

https://doi.org/10.1038/s41467-025-62119-9

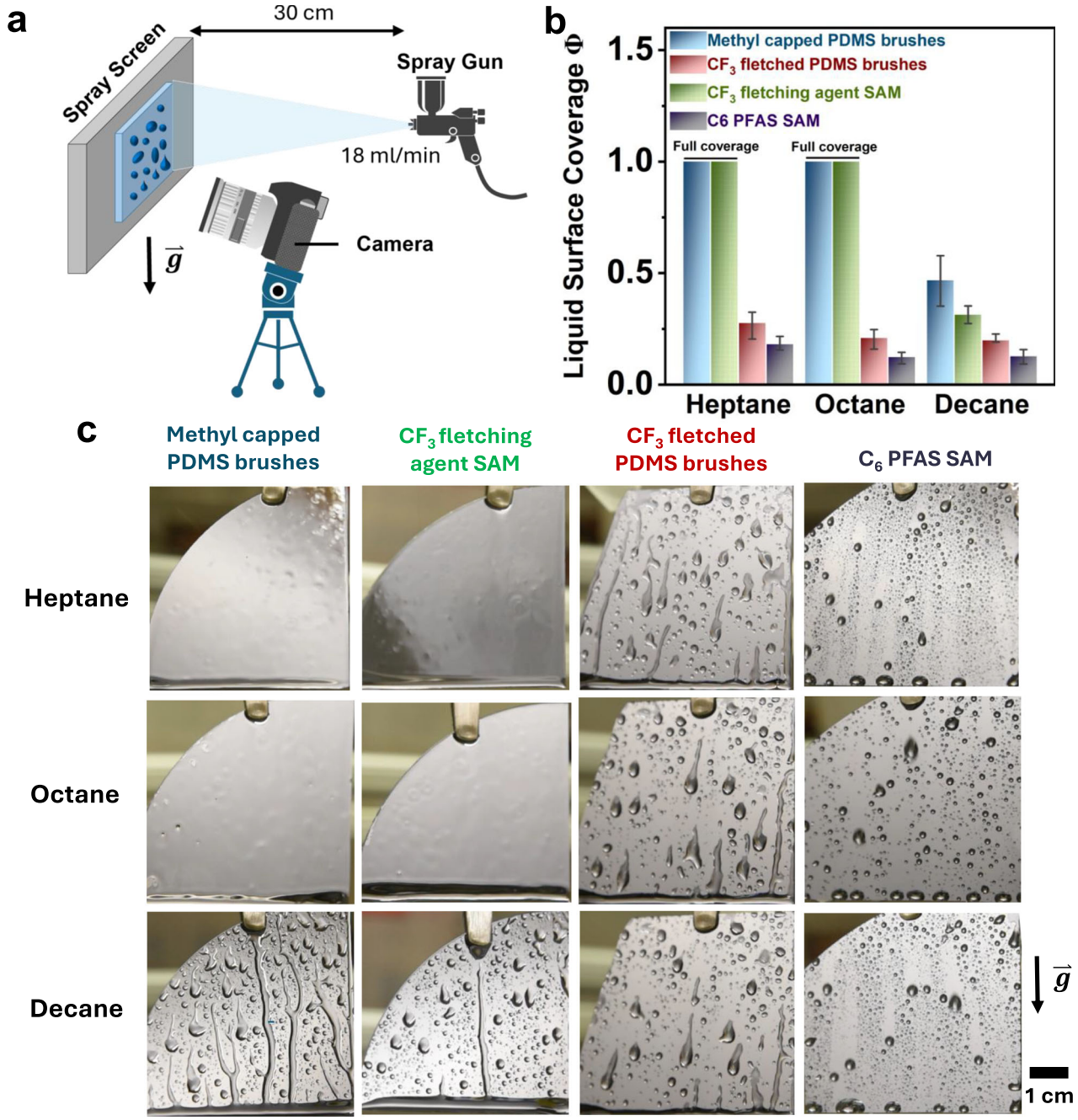

Fig. 4 | Spray test of low surface tension oils. a Schematic illustration of the liquid spray test. **b** Liquid surface coverage Φ for the methyl capped PDMS brushes, CF_3 fletched PDMS brushes, CF_3 fletching agent SAM and C_6 PFAS SAM. Here $N = 5$ and the data is the mean ± 1 std. **c** Droplet visualization during heptane, octane and decane spray at steady state on the methyl capped PDMS brushes, CF_3 fletched PDMS brushes, CF_3 fletching agent SAM and C_6 PFAS SAM. (See Supplementary Movie 1–3).

C4 PFAS coated mesh for various nonpolar liquids (Kaydol 35, hexadecane, tetradecane), which were higher than the meshes coated by methyl capped PDMS brushes and the CF_3 fletching agent SAM. Moreover, there was an abrupt decrease in advancing contact angles between hexadecane and tetradecane on the meshes coated with either the methyl capped PDMS brushes or the CF_3 fletching agent SAM (Fig. 5c). This was caused by a transition from the Cassie-Baxter state to the Wenzel state, where the tetradecane penetrated the mesh pores. These findings suggest that the enhanced oil repellency of the CF_3 fletched PDMS brushes can also be effectively applied to textured surfaces for the enhancement of their capillary resistance, with similar performance to C_4 PFAS.

One industry with immediate need of PFAS replacements is the textile industry, where PFAS-containing fabric finishes impart water, oil, and soiling resistance. Research has shown that the capillary resistance of fibrous materials like fabrics and meshes scales with the tangent of the contact angle, at least for low surface tension fluids like oils. Accordingly, the ~10° higher contact angles exhibited by the CF_3-fletched PDMS brushes, as compared to the methyl capped PDMS brushes or CF_3 fletching agent SAM, should result in higher breakthrough pressures for low surface tension liquids. To further investigate this capillary resistance, 6 μL hexadecane droplets released from increasing heights were used to impact coated meshes until a transition to the Wenzel state was observed, using the static contact angle

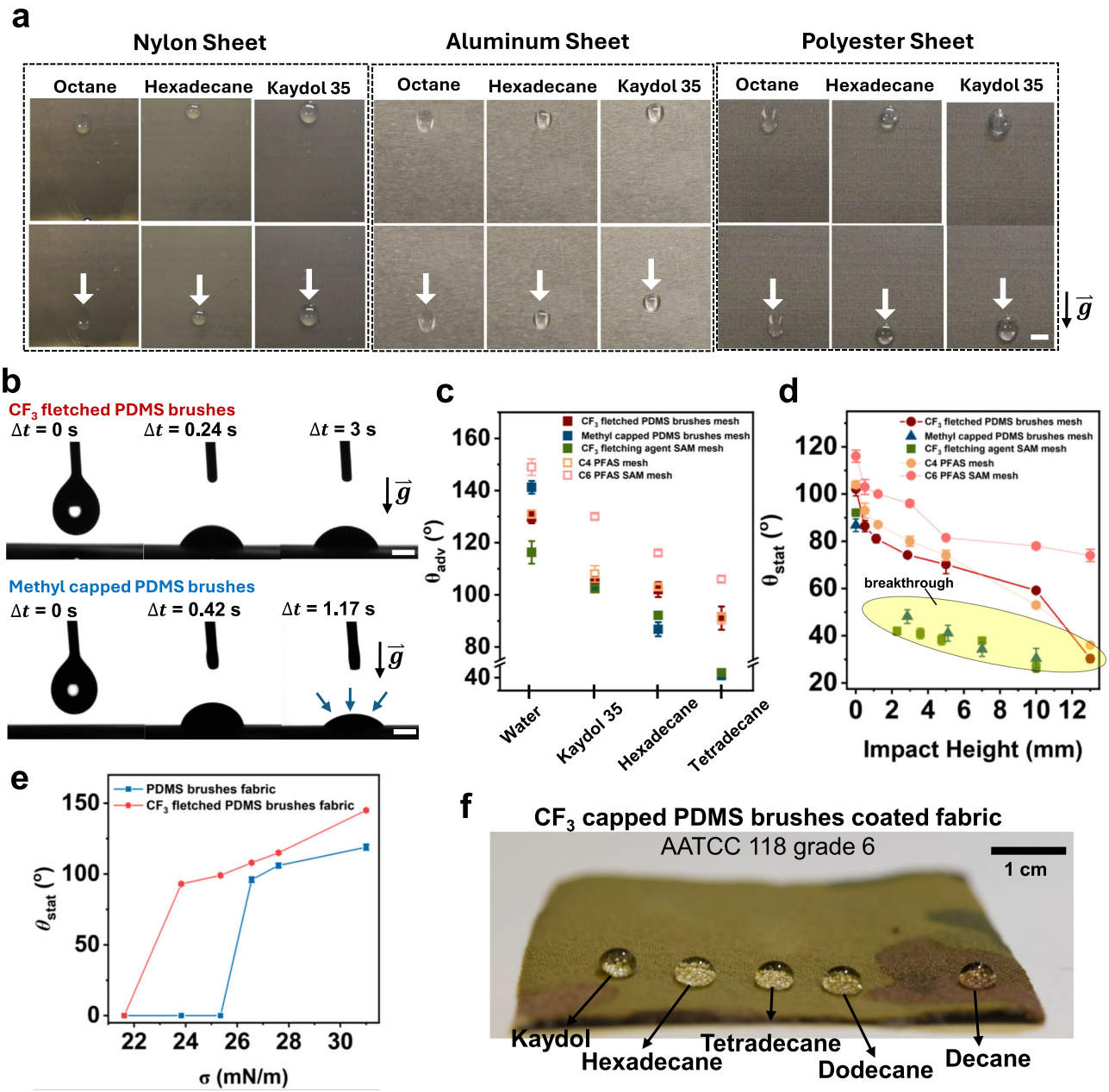

Fig. 5 | Applications of CF_3 fletched PDMS brushes. a Images showing the sliding of octane, hexadecane and Kaydol 35 droplets on a nylon sheet, aluminum sheet, and polyester sheet coated by the CF_3 fletched PDMS brushes. The scale bar is 5 mm. **b** Time-lapsed images of a 6 μL hexadecane droplet impacting meshes coated with either the CF_3 fletched-PDMS brushes or the methyl capped PDMS brushes. The droplet was released from a 1 mm height. Upon impact, the hexadecane droplet was absorbed into the methyl-capped-PDMS-brush coated mesh, as indicated by the blue arrows. The scale bar is 1 mm. **c** Advancing contact angles of water, Kaydol 35, hexadecane, and tetradecane on the meshes coated with the CF_3 fletched PDMS brushes, methyl capped PDMS brushes, the CF_3 fletching agent SAM, C4 PFAS and C6 PFAS SAM. **d** Static contact angles of ~6 μL hexadecane droplets measured after impacting the coated meshes at varying heights. Droplets that absorbed into the meshes are highlighted in yellow. **e** The static contact angles θ_{stat} of Kaydol 35, hexadecane, tetradecane, dodecane, decane and octane measured on the fabrics coated by either PDMS brushes or CF_3 fletched PDMS brushes. For most measurements error is smaller than the presented symbols. In (**c**–**e**), $N = 5$ and the data is the mean ± 1 std. **f** Different low surface tension oils deposited on the CF_3 fletched PDMS brush-coated fabric.

θ_{stat} as a probe (Fig. 5d). Droplet absorption (Cassie-Baxter to Wenzel transition) was observed on the meshes coated with either the methyl-capped PDMS brushes or the CF_3 fletching agent SAM for all droplets released from a height greater than 1 mm. In contrast, the CF_3-fletched-PDMS-brushes coated mesh was able to maintain its Cassie-Baxter state up to an impact height of 11 mm, i.e., capable of resisting at least a Bernoilli pressure of ~84 Pa. Higher impact heights resulted in breakthrough. These breakthrough pressure measurements were also confirmed using liquid columns, where again the pressure resistance of the mesh coated with CF_3-fletched PDMS brushes outperformed the other two coated meshes (Supplementary note 10). As with the dynamic contact angle measurements (Fig. 5c), the CF_3-fletched PDMS brushes performed similarly with the C4 PFAS coated meshes, but exhibited lower capillary resistance than the C_6 PFAS SAM-coated meshes.

To demonstrate a realistic application, we coated a fabric with the CF_3 fletched PDMS brushes and compared its oil repellency to a fabric coated with PDMS brushes only (See Supplementary Methods). We assessed the fabrics using the AATCC 118: Oil Repellency: Hydrocarbon Resistance Test standard (see Supplementary note 11). In Fig. 5e, the static contact angles of the standard test liquids (Kaydol 35,

hexadecane, tetradecane, dodecane, decane and octane) on the fabrics coated with PDMS brushes and CF_3 fletched PDMS brushes are plotted against their surface tension. The static contact angle of all oils tested on the CF_3 fletched PDMS brush-coated fabric was always higher than that on the PDMS brush-coated fabric. Further, fabric coated only with PDMS brushes were wet by the oils with surface tension lower than tetradecane (26.5 mN/m); 0° contact angles were observed for dodecane, decane and octane. Accordingly, the PDMS brush-coated fabric only achieved grade 4 oil repellency. In contrast, the fabric coated with CF_3 fletched PDMS brushes could resist lower surface tension oils, down to decane (23.8 mN/m), achieving grade 6 oil repellency (Fig. 5f).

For practical applications the durability of any surface coating is of critical importance. First, we examined the thermo-oxidative stability of the CF_3 fletched PDMS brushes and compared it with the C_4 PFAS and C_6 PFAS SAM surfaces. The coatings were fabricated on silicon wafers and were heated to 100 °C and 200 °C for 72 h (Supplementary note 12). The results (Supplementary Fig. 12) demonstrate that the contact angles of the CF_3 fletched PDMS brushes remained unchanged after both temperature exposures. Second, we characterized the stability of the coatings under strongly acidic and basic conditions (Supplementary note 12). We found that the CF_3 fletched PDMS brushes could resist acidic environments down to pH 3 for 24 h (Supplementary Fig. 13), though at pH 1 degradation was slightly observed. The CF_3 fletched PDMS brushes here performed more closely to the C_6 PFAS SAM, and outperformed the C_4 PFAS surface. Similar results were observed at pH 10, although at pH 13 all three surfaces were wet by hexadecane, as siloxane bonds are not stable at this pH. Lastly, the CF_3 fletched PDMS brushes were tested against a water jet to demonstrate their resistance to high pressure impact[64]. A water jet with a velocity of 1.3 m/s impacted the surface three times for 5 s (Supplementary note 12). After the water jet impact, the contact angles of water and hexadecane remained the same (Supplementary Fig. 14), similar to the C_4 PFAS and C_6 PFAS SAM surfaces.

Discussion

To provide the oleophobicity currently enabled by short-chain PFAS (C_4 and C_6), but without the associated health and environmental concerns, we explored the application of single perfluorinated groups. When combined with the liquid-like nature of PDMS brushes the surface density of CF_3 groups can be maximized. With a slight increase in reactive sites after a short, 15 s plasma treatment, angle-resolved XPS elucidated that ~7 -CF_3 groups can be bonded along the uppermost portion of the PDMS chains, which simultaneously minimizes both the surface energy and total fluorine within the coating. The total surface energy of the CF_3-fletched PDMS brushes is significantly lower than that of the non-fluorinated PDMS brushes and approaches the surface energy of C_4 and C_6 PFAS. However, this is achieved with 8 times less fluorine than C_6 PFAS and 40 times less fluorine than a C_4 PFAS surface with comparable wettability. Our results demonstrate that incorporating single -CF_3 groups along a PDMS brush can achieve repellency of low surface tension oils comparable to short-chain PFAS without the need for perfluorinated alkyl chains. These results disprove the decades-old belief that the liquid repellency of PFAS is inherently coupled with chain length, and allow for the minimization of surface energy through molecular architecture rather than increasing the length of a perfluorinated chain. However, this begs the question of whether a surface that degrades to by-products such as trifluoroacetic acid is sustainable long-term.

Since the sole fluorinated moiety within the CF_3 fletched PDMS brushes coating is a -CF_3 group, eventual environmental degradation is likely to produce trifluoroacetic acid (TFA) as the terminal by-product from various reaction mechanisms such as hydrogen abstraction by environmental radical hydroxyls[51] or biotransformation pathways[52] (Supplementary note 13). There have been several studies that suggest TFA is non-bioaccumulative and less toxic than PFAS of longer chain length, and have reported negligible or mild effects on mammalian liver, body weight, food consumption and genome mutation from the uptake of TFA[34,65–68]. However, there is still contradicting evidence on whether TFA poses embryo-fetal developmental toxicity in mammals[66,69]. Further, the long-term environmental accumulation of TFA due to its high persistence remains an underlying concern[70] to many researchers and its actual impact is yet unknown. Although a more in-depth study is still required to obtain a thorough understanding of the toxicity of TFA, it is also instructive to place the potential TFA emissions from the CF_3 fletched PDMS brushes into context.

Consider, for example, a waterproof jacket rendered oil repellent using our the CF_3 fletched PDMS brushes. Given the common specific surface area of non-woven fabrics[71] (~ 0.363 m^2/g) and the regular size of a jacket (~283 g), the maximum emission of TFA of the CF_3 fletched PDMS brushes per jacket would be around 65 mg, using the measured fluorine area density of~ 10 F/nm^2. As of 2025, major sources of TFA emissions include hydrofluorocarbon (HFC) refrigerants, pesticides, and pharmaceuticals[34]. The potential emission of TFA from the leakage of the HFC refrigerant R-134a from a vehicle's air conditioning in China in just over an hour (~52.2 mg/hr/vehicle)[72] would almost reach the entire eventual TFA emissions from a jacket coated with CF_3 fletched PDMS brushes. Similarly, pesticides or plant protection products (PPP) also largely contribute to global TFA emissions. By surveying sales data from 2011 to 2017, the average emission of TFA in Germany only arising from the use of PPP is estimated to be 3.5 $kg/km^2/year$[73]. Considering the average size of a farm in Germany (~61 hectares)[74], the average emission of TFA from each farm is 2.14 kg per year and there are around 276,000[74] farms within Germany. This would be equal to the amount of TFA emitted from the complete degradation of 9 trillion jackets annually. Overall, not only could the CF_3 fletched PDMS brushes eliminate longer-chain PFAS emissions, but the emissions from its terminal degradation by-products such as TFA would be negligible compared to other major sources.

Although the CF_3 fletched PDMS brushes appear promising in terms of enhancing oil repellency with minimal fluorination, several challenges remain in terms of real-world scale-up. While in-line plasma treatment systems do exist to achieve the ~15 s plasma activation prior to CF_3 fletching, pre-functionalised monomers might circumvent the need for plasma activation entirely. Siloxane monomers could be pre-reacted with CF_3 side chains, followed by the grafting-from method to synthesize the polymer brushes. However, steric hinderance of the bulky monomer may prevent the graft density required to achieve the polymer brush conformation. More complex and non-planar substrate geometries, such as the internal walls of pipelines or the external surfaces of condensers, might also present scalability issues. On the other hand, we have demonstrated that the current fabrication method is applicable to planar porous and textured substrates, such as metal meshes and synthetic fabrics (Fig. 5).

In conclusion, this work presents an effective design that combines -CF_3 groups with PDMS brushes to repel low surface tension oils without the use of fluorocarbon chains. The PDMS brushes offer an alternate mechanism for maximizing -CF_3 surface density as compared to PFAS, which derives from the flexible, liquid-like nature of PDMS brushes. Such an approach is advantageous during the phasing out of oil-repellent materials that utilize PFAS, and paves the way to a completely PFAS-free future.

Methods

Materials

Silicon wafers (100) were purchased from University Wafer (Boston, MA). Teflon, polyester, polished 6061 aluminum sheets, and a 325 × 325 plain weave stainless-steel mesh were bought from McMaster Carr (Elmhust, IL). Fabric was kindly provided by PRE Labs

Inc (Kelowna, BC). 1,3-dichlorotetramethyldisiloxane, (3,3,3-trifluoropropyl)dimethylchlorosilane, tridecafluorooctyl-dimethylchlorosilane, and nonafluorohexyltriethoxysilane were purchased from Gelest Inc. (Morrisville, PA). Chlorotrimethylsilane 98% and octane were bought from Thermofisher (Waltham, MA). Toluene, heptane and hydrochloric acid (38%) were obtained from VWR (Radnor, PA). 2-Propanol 99.5% was supplied from Fisher Scientific (Hampton, NH). Hexadecane, tetradecane and tetraethoxysilane (TEOS) were ordered from Alfa Aesar (Ward Hill, MA). Dodecane was purchased from Sigma Aldrich. Decane was purchased from Fisher Scientific.

Cleaning of silicon wafers

Silicon wafers were first rinsed in toluene and 2-propanol for 30 s and dried under compressed air. After washing, the silicon wafers were treated with oxygen plasma (PDC-FMG, Harrick Plasma) for 2 min at 400 mTorr vacuum pressure under RF power of 45 W.

Preparation of PDMS brushes

Plasma treated silicon wafers were placed in a petri dish with 2 glass vials each containing 100 μL of 1,3-dichlorotetramethyldisiloxane under relative humidity of 20% in room temperature. The lid of the petri dish was then added, allowing the reaction to proceed for 5 min. Next, the silicon wafer was removed from the petri dish and rinsed by toluene and 2-propanol followed by drying under compressed air.

Preparation of CF_3 fletched PDMS brushes

The PDMS brushes were first treated with oxygen plasma for surface activation under a vacuum pressure of ~350 mTorr and RF power of 30 W. The plasma treatment times were 0 s (no treatment), 3 s, 5 s, 10 s, 15 s, 20 s and 30 s. After the plasma treatment, the sample was placed in a vacuum chamber with 2 glass vials each containing 100 μL of 3,3,3-trifluoropropyl)dimethylchlorosilane. The chamber was depressurized to 0.1 bar to remove excessive water vapor and then the reaction was allowed to proceed for 2 h. Following this, the sample was removed from the vacuum chamber and rinsed with toluene and 2-propanol to remove unreacted silane followed by drying under compressed air.

Preparation of methyl capped PDMS brushes

PDMS brush-coated wafers were placed in a petri dish with 2 glass vials each containing 100 μL of chlorotrimethylsilane, and then the lid of the petri dish was put on. The sample was removed from the closed petri dish after 2 h of reaction and then rinsed with toluene and 2-propanol for 30 s.

Preparation of CF_3 fletching agent SAM

Plasma-treated silicon wafers were placed in a closed petri dish with 2 glass vials each containing 100 μL of (3,3,3-trifluoropropyl)dimethylchlorosilane. The reaction last for 2 h. After coating, the sample was removed from the petri dish and rinsed with toluene and 2-propanol to remove unreacted silane followed by drying under compressed air

Preparation of C_6 PFAS SAM

Plasma-treated silicon wafers were placed in an airtight glass container containing 2 glass vials of 100 μL of tridecafluorooctyldimethylchlorosilane. The container was then placed in a 120 °C oven for vapor deposition for 2 h. Following this, the sample was removed from the container after the reaction completed and was subsequently washed in toluene and 2-propanol followed by drying under compressed gas.

Preparation of C_4 PFAS SAM

Plasma-treated silicon wafers were placed in an airtight glass container containing 2 glass vials of 100 μL of nonafluorohexyltriethoxysilane and the container was then placed in a 120 °C oven for vapor deposition for 2 h. Following this, the sample was removed from the container and was washed in toluene and 2-propanol followed by drying under compressed gas.

Preparation of pre-reaction of CF_3 fletching agent with PDMS oil (4200 $gmol^{-1}$ and 26,000 $gmol^{-1}$) for XPS studies

0.5 g of each PDMS oil was diluted in 19.5 g of toluene. Next, 22.7 mg and 3.7 mg of 3,3,3-trifluoropropyldimethylchlorosilane were added to PDMS oil (4200 $gmol^{-1}$) solution and PDMS (26,000 $gmol^{-1}$) solution respectively. Both solution were allowed to react for 24 h. Plasma-treated silicon wafers were then coated with the solution via spin-coating at 1500 rpm for 1 min, followed by curing in a 120 °C oven for 15 min. Next, the coated silicon wafer was washed in toluene and 2-propanol to remove any unbonded PDMS oil and unbonded CF_3 fletching agent molecules. Following this, an additional vapor deposition of CF_3 fletching agent was performed to eliminate any residual silanols groups. Two vials containing 100 μL of CF_3 fletching agent were placed with the coated silicon wafer in a closed petri dish to do this. The reaction lasted for 1 h, followed by washing in isopropyl alcohol and toluene.

Preparation of CF_3 fletched PDMS brush coating on aluminum, polyester, and nylon substrates

The substrates were first cut into pieces of size 3 cm × 4 cm and washed in hexane and 2-propanol for 30 s, followed by drying using compressed air. Next, the substrates were treated with oxygen plasma using a vacuum pressure of 400 mTorr and RF power of 45 W for 2 min. To fabricate a thin silica layer on the substrates, a TEOS solution was prepared as described in Ref. 1, where TEOS/ethanol/H_2O/HCl were mixed in a mole ratio of 1/3.8/6.4/0.085. First, ethanol and TEOS were mixed and stirred at room temperature for 1 min at 600 rpm. Then, water and HCl were added and the solution temperature was raised to 60 °C. The solution was then allowed to react for 3 h at 60 °C under constant stirring. After the reaction, the solution was cooled to room temperature and aged for 1 day before being used. The diluted TEOS solution was spin-coated on the plasma treated substrates at 3000 rpm for 30 s. The coated substrate was then placed on an 80 °C hot plate for 1 h. After coating the substrate with silica, the CF_3 fletched PDMS brushes were fabricated on the silica layer using the same methods as described above.

Preparation of stainless-steel mesh and fabric for coating

Each substrate was cut into pieces of size 2 cm × 2 cm and washed in toluene and 2-propanol for 30 s, and was then dried using compressed air. Next, the substrate was treated with oxygen plasma at a vacuum pressure of 400 mTorr and RF power of 45 W for 10 min to remove organic contaminants and increase the reactivity of the surface. To fabricate a thin silica layer on the meshes or fabric, the plasma treated substrate was immersed in a 20 times diluted TEOS solution for 30 min and dried in a 120 °C oven for 15 min of curing[2]. Finally, the silica-coated substrate was coated with either CF_3 fletched PDMS brushes, methyl capped PDMS brushes or the CF_3 fletching agent SAM using the same methods as described above.

Atomic force microscope. Surface topology and roughness measurements were conducted using an Asylum Cypher Atomic Force Microscope (Oxford Instruments, Santa Barbara, USA) operating in tapping mode with a Point Probe Plus sharp silicon cantilever (Nanosensors, Neuchatel, Switzerland). Each surface was imaged at three locations across 1 × 1 μm scan regions with 512 pixels at a scan rate of 1 Hz, and the root-mean-squared roughness S_{rms} was calculated using MATLAB.

X-ray photoelectron spectroscopy. X-ray photoelectron spectroscopy (XPS) data was obtained from a K-Alpha X-ray Photoelectron Spectrometer (XPS) System with a monochromatic, microfocused Al

K-Alpha X-ray source. The analyzed region was a circle with radius of 150 μm. The experiment was carried out at a pressure of 10^{-8} Pa during the experiments and the results were analyzed by the Avantage Data System.

Total organic fluorine – combustion ion chromatography. Samples were analyzed for total fluorine concentration by combustion ion chromatography (CIC). The CIC system comprised an automatic boat controller (ABC), water vapor injection module (WS-100), automatic quick furnace (AQF-100), gas absorption unit (GA-100), and Dionex ICS-2100 ion chromatography system. PFAS-coated samples with known accurate mass were first placed on a pre-cleaned quartz glass sample boat and introduced to the combustion furnace using the programmable automatic boat controller. The combustion furnace operated at a temperature range of 900 °C to 1000 °C at the entrance and exit of the furnace, respectively. Samples were combusted in the presence of argon (200 mL/min, 6.0 purity). Ultrapure water was added at a rate of 0.1 mL/min to the argon gas stream to promote hydropyrolysis. Total sample combustion time was 10 min, with oxygen introduced during the final 3 min of combustion at a rate of 400 mL/min (5.0 purity). During this process all organofluorine was converted to HF. Combustion gasses were bubbled through an aqueous bubbler containing 5 mL of 10 mM potassium hydroxide solution. The concentration of fluoride in each sample solution was determined by ion chromatography.

Contact angle measurement. Contact angles were measured using a Ramé-hart goniometer (Model 260-U4). A 5 μL droplet of the probe liquid was first deposited onto the sample from a micropipette. The static contact angle was measured when the needle was removed from the droplet. Additional liquid was added to the stationary droplet by reinserting the dispenser needle to the droplet until the contact line started to move outward and the advancing contact angle was measured at this moment. In contrast, the receding contact angle was measured when the liquid was withdrawn from the droplet and the contact line stated to move inward. The contact angles were analysed using the Ramé-hart DROPimage software and at least five measurements were performed on spatially different locations of each sample surface. The contact angle hysteresis was calculated by the difference of the advancing contact angle and the receding contact angle.

Measurement of PDMS brushes thickness. The thickness of the PDMS brushes coated on the silicon wafer was measured by a Film Sense FS-8 ellipsometer at eight wavelengths from 370 to 950 nm. The incident angle was set to 70°. The measurement was performed by setting a two-layer model which was comprised of a substrate layer: silicon with its native oxide of known thickness (1.9 nm), and the PDMS brush layer to be fitted by the Cauchy Model for transparent materials. The thickness of the PDMS brushes was measured on at least five different spots on the sample surface to obtain an average.

Data availability

All data are available from the corresponding author upon request. The source data are available at https://doi.org/10.6084/m9.figshare.29217989.

References

1. Jiao, L. et al. Facile preparation of pliable superamphiphobic papers with high and durable liquid repellency for anti-corrosion and open surface microfluidics. *Appl. Surf. Sci.* **606**, 154845 (2022).
2. Li, C. et al. Under oil open-channel microfluidics empowered by exclusive liquid repellency. *Sci. Adv.* **6**, eaay9919 (2020).
3. Fazle Rabbi, K. et al. Polydimethylsiloxane-silane synergy enables dropwise condensation of low surface tension liquids. *Adv. Funct. Mater.* **32**, 2112837 (2022).
4. Boylan, D. et al. Patterned Quasi-liquid surfaces for condensation of low surface tension fluids. *Adv. Funct. Mater.* **34**, 2400194 (2024).
5. Cha, H. et al. Dropwise condensation on solid hydrophilic surfaces. *Sci. Adv.* **6**, eaax0746 (2020).
6. Yang, J. et al. Janus membranes with controllable asymmetric configurations for highly efficient separation of oil-in-water emulsions. *J. Mater. Chem. A Mater.* **7**, 7907–7917 (2019).
7. Brown, P. S., Atkinson, O. D. L. A. & Badyal, J. P. S. Ultrafast oleophobic–hydrophilic switching surfaces for antifogging, self-cleaning, and oil–water separation. *ACS Appl. Mater. Interfaces* **6**, 7504–7511 (2014).
8. Li, J. et al. Simple preparation method for hydrophilic/oleophobic coatings. *ACS Appl. Mater. Interfaces* **12**, 45266–45273 (2020).
9. Zhao, H. et al. Extreme antiscaling performance of slippery omniphobic covalently attached liquids. *ACS Appl. Mater. Interfaces* **12**, 12054–12067 (2020).
10. Sin, D. T. et al. Multifunctional oil-entangled matrix spray for maritime sustainability. *Adv. Mater. Technol.* **8**, 2300839 (2023).
11. Yan, X. et al. Unraveling the role of vaporization momentum in self-jumping dynamics of freezing supercooled droplets at reduced pressures. *Nat. Commun.* **15**, 1567 (2024).
12. Jin, P. et al. Ultra-low ice-substrate adhesion and self-deicing during droplet impact freezing. *Cell Rep. Phys. Sci.* **3**, 100894 (2022).
13. Jiang, J. et al. An energy-free strategy to elevate anti-icing performance of superhydrophobic materials through interfacial airflow manipulation. *Nat. Commun.* **15**, 777 (2024).
14. Ateia, M., Maroli, A., Tharayil, N. & Karanfil, T. The overlooked short- and ultrashort-chain poly- and perfluorinated substances: a review. *Chemosphere* **220**, 866–882 (2019).
15. Zenasni, O., Jamison, A. C. & Lee, T. R. The impact of fluorination on the structure and properties of self-assembled monolayer films. *Soft Matter.* **9**, 6356 (2013).
16. Nishino, T., Meguro, M., Nakamae, K., Matsushita, M. & Ueda, Y. The lowest surface free energy based on $-CF_3$ alignment. *Langmuir* **15**, 4321–4323 (1999).
17. Demir, T. et al. Toward a long-chain perfluoroalkyl replacement: water and oil repellency of Polyethylene Terephthalate (PET) films modified with perfluoropolyether-based polyesters. *ACS Appl. Mater. Interfaces* **9**, 24318–24330 (2017).
18. Björnsdotter, M. K., Yeung, L. W. Y., Kärrman, A. & Ericson Jogsten, I. Challenges in the analytical determination of ultra-short-chain perfluoroalkyl acids and implications for environmental and human health. *Anal. Bioanal. Chem.* **412**, 4785–4796 (2020).
19. Guzman-Puyol, S. et al. Greaseproof, hydrophobic, and biodegradable food packaging bioplastics from C6-fluorinated cellulose esters. *Food Hydrocoll.* **128**, 107562 (2022).
20. Chang, S.-C. et al. Thyroid hormone status and pituitary function in adult rats given oral doses of perfluorooctanesulfonate (PFOS). *Toxicology* **243**, 330–339 (2008).
21. Olsen, G. W. et al. A comparison of the pharmacokinetics of perfluorobutanesulfonate (PFBS) in rats, monkeys, and humans. *Toxicology* **256**, 65–74 (2009).
22. Gannon, S. A. et al. Absorption, distribution, metabolism, and excretion of [1-14C]-perfluorohexanoate ([14C]-PFHx) in rats and mice. *Toxicology* **283**, 55–62 (2011).
23. *ANSES. Development of Oral-Administrated Treatment for TRV by Perfluorohexanoic Acid (PFHxA).* https://www.anses.fr/fr/system/files/SUBSTANCES2015SA0129EN.pdf (2017).
24. USEPA. *Health Effects Support Document for Perfluorooctanoic Acid (PFOA).* https://www.epa.gov/sites/production/files/2016-05/ (2016).
25. Luz, A. L., Anderson, J. K., Goodrum, P. & Durda, J. Perfluorohexanoic acid toxicity, part I: development of a chronic human health toxicity value for use in risk assessment. *Regulat. Toxicol. Pharmacol.* **103**, 41–55 (2019).

26. Kjolholt, J., Jensen, A. A. & Warming, M. *Short-Chain Polyfluoroalkyl Substance (PFAS)*. A literature review of information on human health effects and environmental fate and effect aspects of short-chain PFAS. https://www2.mst.dk/Udgiv/publications/2015/05/978-87-93352-15-5.pdf. (2015).
27. Chemicals Strategy for Sustainability Towards a Toxic-Free Environment. https://ec.europa.eu/environment/pdf/chemicals/2020/10/SWD_PFAS.pdf.
28. Shabanian, S., Lahiri, S. K., Soltani, M. & Golovin, K. Durable water- and oil-repellent textiles without long- or short-chain perfluoroalkylated substances. *Mater. Today Chem.* **34**, 101786 (2023).
29. Chen, L., Huang, S., Ras, R. H. A. & Tian, X. Omniphobic liquid-like surfaces. *Nat. Rev. Chem.* **7**, 123–137 (2023).
30. Soltani, M. & Golovin, K. Lossless, passive transportation of low surface tension liquids induced by patterned omniphobic liquidlike polymer brushes. *Adv. Funct. Mater.* **32**, 2107465 (2022).
31. Rajabi-Abhari, A., Soltani, M., Golovin, K. & Yan, N. Nature-inspired surface for simultaneously harvesting water and triboelectric energy from ambient humidity using polymer brush coatings. *Nano Energy* **115**, 108752 (2023).
32. Urata, C., Masheder, B., Cheng, D. F. & Hozumi, A. Unusual dynamic dewetting behavior of smooth perfluorinated hybrid films: potential advantages over conventional textured and liquid-infused perfluorinated surfaces. *Langmuir* **29**, 12472–12482 (2013).
33. Park, J., Urata, C., Masheder, B., Cheng, D. F. & Hozumi, A. Long perfluoroalkyl chains are not required for dynamically oleophobic surfaces. *Green. Chem.* **15**, 100–104 (2013).
34. Garavagno, M. et al. Trifluoroacetic acid: toxicity, sources, sinks and future prospects. *Sustainability* **16**, 2382 (2024).
35. Liu, J. et al. Successful trifluoromethoxy-containing pharmaceuticals and agrochemicals. *J. Fluor. Chem.* **257–258**, 109978 (2022).
36. Yao, C. et al. Fluorination of a polymer donor through the trifluoromethyl group for high-performance polymer solar cells. *J. Mater. Chem. A Mater.* **8**, 12149–12155 (2020).
37. Schill, H. et al. 4-Trifluoromethyl-substituted coumarins with large stokes shifts: synthesis, bioconjugates, and their use in super-resolution fluorescence microscopy. *Chem. – A Eur. J.* **19**, 16556–16565 (2013).
38. Khatir, B., Azimi Dijvejin, Z., Serles, P., Filleter, T. & Golovin, K. Molecularly capped omniphobic polydimethylsiloxane brushes with ultra-fast contact line dynamics. *Small* **19**, e2301142 (2023).
39. Shabanian, S., Khatir, B., Nisar, A. & Golovin, K. Rational design of perfluorocarbon-free oleophobic textiles. *Nat. Sustain.* **3**, 1059–1066 (2020).
40. Hegner, K. I., Hinduja, C., Butt, H.-J. & Vollmer, D. Fluorine-free super-liquid-repellent surfaces: pushing the limits of PDMS. *Nano Lett.* **23**, 3116–3121 (2023).
41. Wong, W. S. Y. et al. Design of fluoro-free surfaces super-repellent to low-surface-tension liquids. *Adv. Mater.* **35**, e2300306 (2023).
42. Song, J. et al. Hierarchically branched siloxane brushes for efficient harvesting of atmospheric water. *Small* **19**, e2301561 (2023).
43. Zhao, X. et al. Macroscopic evidence of the liquidlike nature of nanoscale polydimethylsiloxane brushes. *ACS Nano* **15**, 13559–13567 (2021).
44. Yi, Z. et al. Dual-interface engineering induced by silane coupling agents with different functional groups constructing high-performance flexible perovskite solar cells. *Chem. Eng. J.* **469**, 143790 (2023).
45. Hozumi, A., Ushiyama, K., Sugimura, H. & Takai, O. Fluoroalkylsilane monolayers formed by chemical vapor surface modification on hydroxylated oxide surfaces. *Langmuir* **15**, 7600–7604 (1999).
46. Drelich, J. & Miller, J. D. Modification of the Cassie equation. *Langmuir* **9**, 619–621 (1993).
47. Bodas, D. & Khan-Malek, C. Hydrophilization and hydrophobic recovery of PDMS by oxygen plasma and chemical treatment—An SEM investigation. *Sens Actuators B Chem.* **123**, 368–373 (2007).
48. Khatir, B. et al. Molecular Structure of Omniphobic, Surface-Grafted Polydimethylsiloxane Chains. *Small* https://doi.org/10.1002/smll.202406089 (2024).
49. Colorado, R. & Lee, T. R. Wettabilities of self-assembled monolayers on gold generated from progressively fluorinated alkanethiols. *Langmuir* **19**, 3288–3296 (2003).
50. Yuan, Y., Burgess, J., Volchek, K. & Brown, C. E. Short-Chain PFAS. in *Perfluoroalkyl Substances in the Environment* (eds. Kempisty, D. M., Xing, Y. & Racz, L.) 252–253 (CRC Press, 2018).
51. Dooley, M. R. et al. Atmospheric oxidation of PFAS by hydroxyl radical: a density functional theory study. *ACS EST Air* **1**, 1352–1361 (2024).
52. Rand, A. A., Rooney, J. P., Butt, C. M., Meyer, J. N. & Mabury, S. A. Cellular Toxicity associated with exposure to Perfluorinated Carboxylates (PFCAs) and their metabolic precursors. *Chem. Res Toxicol.* **27**, 42–50 (2014).
53. Joanny, J. F. & de Gennes, P. G. A model for contact angle hysteresis. *J. Chem. Phys.* **81**, 552–562 (1984).
54. Lyu, S., Yang, Z. & Duan, Y. The sliding mode and dissipative force of moving nanodroplets on smooth and striped hydrophobic surfaces. *J. Mol. Liq.* **346**, 118284 (2022).
55. Snoeijer, J. H. & Andreotti, B. Moving contact lines: scales, regimes, and dynamical transitions. *Annu. Rev. Fluid Mech.* **45**, 269–292 (2013).
56. de Gennes, P. G. Wetting: statics and dynamics. *Rev. Mod. Phys.* **57**, 827–863 (1985).
57. Backholm, M. et al. Water droplet friction and rolling dynamics on superhydrophobic surfaces. *Commun. Mater.* **1**, 64 (2020).
58. Li, X. et al. Kinetic drop friction. *Nat. Commun.* **14**, 4571 (2023).
59. Li, X. et al. Spontaneous charging affects the motion of sliding drops. *Nat. Phys.* **18**, 713–719 (2022).
60. Khalil, K. et al. Grafted nanofilms promote dropwise condensation of low-surface-tension fluids for high-performance heat exchangers. *Joule* **3**, 1377–1388 (2019).
61. El Fil, B., Kini, G. & Garimella, S. A review of dropwise condensation: theory, modeling, experiments, and applications. *Int. J. Heat. Mass Transf.* **160**, 120172 (2020).
62. Khatir, B., Shabanian, S. & Golovin, K. Design and high-resolution characterization of silicon wafer-like omniphobic liquid layers applicable to any substrate. *ACS Appl. Mater. Interfaces* **12**, 31933–31939 (2020).
63. Yanagisawa, T., Shimizu, T. & Fukuta, M. Foaming characteristics of an oil-refrigerant mixture. *Int. J. Refrig.* **14**, 132–136 (1991).
64. Liu, J. et al. One-step synthesis of a durable and liquid-repellent Poly(dimethylsiloxane) coating. *Adv. Mater.* **33**, e2100237 (2021).
65. Dekant, W. & Dekant, R. Mammalian toxicity of trifluoroacetate and assessment of human health risks due to environmental exposures. *Arch. Toxicol.* **97**, 1069–1077 (2023).
66. ECHA. *European Chemical Agency: Registration Dossier for Trifuoroacetic Acid*. https://echa.europa.eu/de/registration-dossier/-/registered-dossier/5203/7/1 (2022).
67. Bayers C. *Summary of Toxicological and Metabolism Studies for Furtamone*. https://www.bayer.com/sites/default/files/M-482307-01-5.PDF (2014).
68. EFSA. *European Food Safety, Authority: Reasoned Opinion on the Setting of MRL's for Saflufenacil in Various Crops, Considering the Risk Related to the Metabolite Trifluoroacetic Acid (TFA)*. (2014).
69. ECHA. *Registry of CLH Intentions until Outcome-Sodium Trifluoroacetate and Other Inorganic Salts of Trifluoroacetic Acid*. (2024).
70. Hanson, M. L., Madronich, S., Solomon, K., Sulbaek Andersen, M. P. & Wallington, T. J. Trifluoroacetic acid in the environment:

consensus, gaps, and next steps. *Environ. Toxicol. Chem.* **43**, 2091–2093 (2024).
71. Tascan, M., Vaughn, E. A., Stevens, K. A. & Brown, P. J. Effects of total surface area and fabric density on the acoustical behavior of traditional thermal-bonded highloft nonwoven fabrics. *J. Text. Inst.* **102**, 746–751 (2011).
72. Zhang, Y. et al. Leakage Rates of Refrigerants CFC-12, HCFC-22, and HFC-134a from operating mobile air conditioning systems in Guangzhou, China: tests inside a busy urban tunnel under hot and humid weather conditions. *Environ. Sci. Technol. Lett.* **4**, 481–486 (2017).
73. Joerss, H. et al. Pesticides can be a substantial source of trifluoroacetate (TFA) to water resources. *Environ. Int.* **193**, 109061 (2024).
74. Agricultural and rural development. Germany - CAP Strategic Plan. https://agriculture.ec.europa.eu/cap-my-country/cap-strategic-plans/germany_en.

Acknowledgements

The authors acknowledge that this work was conducted at the University of Toronto, on the traditional lands of the Huron-Wendat, the Seneca and the Mississauga of the Credit. K.G. acknowledge funding from the Canada Foundation for Innovation, through grant no. 41543, and the Natural Sciences & Engineering Research Council, through grants RGPIN-2018-04272 and ALLRP 590792 – 23.

Author contributions

S.A. designed and performed all experiments and wrote the manuscript; J.R.G. and S.A. performed the combustion-ion chromatography; B.K. performed the atomic force microscope measurement; T.F. and S.M. provided advice on the experiments and reviewed the manuscript; K.G. conceived the research, designed experiments and wrote the manuscript.

Competing interests

The authors declare no competing interests.

Additional information

Supplementary information The online version contains supplementary material available at https://doi.org/10.1038/s41467-025-62119-9.

Correspondence and requests for materials should be addressed to Kevin Golovin.

Peer review information *Nature Communications* thanks Jing Hua, Jie Liu, and Xuelin Tian for their contribution to the peer review of this work. A peer review file is available.